Nanoscale

Accepted Manuscript

This is an *Accepted Manuscript*, which has been through the RSC Publishing peer review process and has been accepted for publication.

Accepted Manuscripts are published online shortly after acceptance, which is prior to technical editing, formatting and proof reading. This free service from RSC Publishing allows authors to make their results available to the community, in citable form, before publication of the edited article. This *Accepted Manuscript* will be replaced by the edited and formatted *Advance Article* as soon as this is available.

To cite this manuscript please use its permanent Digital Object Identifier (DOI®), which is identical for all formats of publication.

More information about *Accepted Manuscripts* can be found in the **Information for Authors**.

Please note that technical editing may introduce minor changes to the text and/or graphics contained in the manuscript submitted by the author(s) which may alter content, and that the standard **Terms & Conditions** and the **ethical guidelines** that apply to the journal are still applicable. In no event shall the RSC be held responsible for any errors or omissions in these *Accepted Manuscript* manuscripts or any consequences arising from the use of any information contained in them.

Cite this: DOI: 10.1039/c0xx00000x

www.rsc.org/xxxxxx

ARTICLE TYPE

Pitaya-like Sn@C nanocomposite as high-rate and long-life anode for lithium-ion batteries

Ning Zhang, Qing Zhao, Xiaopeng Han, Jingang Yang, and Jun Chen*

Received (in XXX, XXX) Xth XXXXXXXXX 20XX, Accepted Xth XXXXXXXXX 20XX

DOI: 10.1039/b000000x

In this article, we report on the preparation of pitaya-like Sn@C nanocomposite with an aerosol spray pyrolysis and the application as high-rate and long-life anode material of lithium-ion batteries. The structure and morphology analysis of the as-prepared Sn@C nanocomposite shows that Sn nanoparticles with the size of about 8 nm are homogeneously dispersed in the spherical carbon matrix (denoted as Sn8@C). The capacity of Sn8@C nanocomposite exhibits 1007.1 mA h g^{-1} in the initial discharge and maintains the reversible capacity of 910 mA h g^{-1} after 180 cycles at 200 mA g^{-1} (0.305 C). A capacity of 410 mA h g^{-1} was obtained after 1000 cycles at 4000 mA g^{-1} (6.1 C). Furthermore, Sn8@C nanocomposite displays a charge/discharge capacity of 205.3 mA h g^{-1} at 16000 mA g^{-1} (24.4 C). This high-rate performance is owing to that the ultrasmall tin nanoparticles can effectively alleviate the absolute stress/strain during lithiation/delithiation process and that the uniformly embedded nanoparticles in the stable carbon framework can accommodate the large volume change with a buffering effect to prevent Sn nanoparticles from aggregation.

Introduction

Metallic Sn has been proved as a promising anode material for lithium-ion batteries (LIBs) due to its high lithium-ion storage capacity and low charge–discharge potentials.[1-7] The theoretical specific capacity of Sn to $Li_{4.4}Sn$ is 992 mA h g^{-1}, which is much higher than that of graphite (372 mA h g^{-1}).[8-13] However, the serious volume change between Sn and $Li_{4.4}Sn$ is about 300%, leading to the pulverization of the active particles and then poor cycling life. To address this problem, a general method is to use Sn-M or Sn-M-C alloys (M = Ni[14-17], Co[18], Fe[19], or Mn[20]), where M is an inactive confining buffer that can absorb the large volume change. In this case, the energy capacity is decreased because of the existence of the inactive components. Recently, two main effective strategies have been applied to enhance the electrochemical behaviour of Sn anode. One way is to reduce the particle size of Sn to nanoscale.[5, 21] It is found that nanosized Sn particles can endure much higher strain and effectively mitigate the pulverization of the active materials. However, nanosized particles tend to aggregate during the electrochemical alloying-dealloying process, resulting in the inevitable capacity decay. The other method is to integrate nano-Sn with a conductive matrix such as carbon,[10, 22-25] which can relieve mechanical stress and accommodate volume expansion for keeping the integrity of the electrode. For example, Sn nanoparticles with the size of about 30 nm encapsulated in carbon matrix delivered a discharge capacity of 500 mA h g^{-1} after 200 cycles.[5] Sponge-like porous Sn/C composite, which was synthesized by dispersing SnO_2 nanoparticles in a polymer matrix with subsequent carbonization, showed an improved electrochemical behaviour as an anode of LIBs.[23] It is also noted that large amounts of void space in Sn-based porous/hollow composite[26, 27, 28] could accommodate the volume change, but the volumetric capacity is decreased to some extent due to the porous/hollow structure with low tapping density.

Recently, an aerosol assisted method has attracted a great attention to synthesize various materials, benefiting from its rapid reaction, large scale, and continuous production.[22, 29-34] Particularly, Sn/C nanocomposites were successfully prepared by this method. Archer and co-workers synthesized hierarchical carbon particles with the encapsulation of ~15 nm Sn using aerosol assisted method.[29] The as-prepared Sn-C and Sn-$C_{Pluronic}$ showed a capacity of 470 and 640 mA h g^{-1} after 200 cycles respectively. The initial coulombic efficiency for Sn-C and Sn-$C_{Pluronic}$ were 40% and 30%, respectively. Wang's group had prepared nano-Sn/C composite through the robust method.[22] A reversible capacity of 710 mA h g^{-1} was kept after 130 cycles. The general aerosol approaches usually employ surfactants as a template to control the morphology and a diffusion dryer to absorb the solvent.[33]

In this study, we synthesize pitaya-like Sn@C nanocomposite with ~8 nm Sn nanoparticles uniformly dispersed in a carbon matrix using an aerosol spray pyrolysis method. We develop a simple, low cost and surfactants-free method without a diffusion dryer to prepare Sn@C nanocomposite. Briefly, we use $SnCl_2 \cdot 2H_2O$ and resorcinol formaldehyde (RF) resin solution as tin and carbon sources, respectively. In the precursor solution, the RF polymer, which carries negative charges,[35] can effectively coat Sn^{2+}. During the spraying by constant output atomizer, the precursor solution can generate small droplets continuously, and then carbonize RF and reduce Sn^{2+} simultaneously in the inert atmosphere furnace. Furthermore, the size of the embedded Sn grains could be varied by changing the mass of tin and carbon sources. The as-prepared uniform Sn@C spherical nanocomposite displayed an initial discharge capacity of 1007.1 mA h g^{-1} with a coulombic efficiency of 63.3%. Remarkably, it further showed a high-rate capability of 205.3 mA h g^{-1} at 16000 mA g^{-1} (24.4 C) and a reversible capacity of 410 mA h g^{-1} at 4000

mA g^{-1} (6.1 C) after 1000 cycles.

Experimental

Synthesis of pitaya-like Sn@C nanocomposite with different Sn size. Spherical Sn@C nanocomposite was prepared using an aerosol spray pyrolysis technique, which is schematically shown in Fig. S1. After exploring reaction factors such as reaction temperature, gauge pressure and precursor concentration, the optimal conditions were fixed up to synthesize Sn@C nanocomposite with Sn particle size of ~8 nm (denoted as Sn8@C) (Fig. S2). The preparation process involves the following process. (1) 7.7 g resorcinol and 10 ml formaldehyde were prepolymerized in advance to form a solution at room temperature; (2) the resorcinol formaldehyde (RF) resin solution and 6.768 g $SnCl_2$•$2H_2O$ were dissolved into 290 ml ethanol, stirring to prepare homogeneous clear solution; (3) The precursor solution was sprayed with argon flow by a constant output atomizer (Model 3076, TSI, Inc.) and the gauge pressure was 0.2 MPa. The aerosols subsequently passed through a cannular reactor (2.54 cm (ID) × 80 cm (L)) within tubular furnace at 800 °C for residence time about 1-2 s. The final product was collected on a small quartz tube (2.5 cm (ID) ×2.0 cm (L)), which was placed at the end of the reactor. In comparison, spherical Sn@C composite with 40 nm diameter of Sn nanoparticles (labeled as Sn40@C) was obtained by just altering the mass of $SnCl_2$•$2H_2O$, resorcinol, formaldehyde and ethanol to 33.84 g, 9.24 g, 12 ml and 285 ml, respectively.

Material characterizations. The crystalline structure and morphologies of the as-prepared samples were characterized by X-ray diffraction (XRD, Rigaku MiniFlex600, Cu Kα radiation), feld-emission scanning electron microscopy (SEM, JEOL JSM7500F) and transmission electron microscopy (TEM, Philips Tecnai-F20).[36, 37] Thermogravimetric analysis (TGA) was carried out to test the carbon content of Sn8@C and Sn40@C using a TG-DSC analyzer (NETZSCH, STA 449 F3) with a heating rate of 5 °C/min in air from room temperature to 700 °C.

Electrochemical measurements. The Sn@C anode was fabricated by mixing 70% Sn@C composite, 15% carboxymethyl cellulose (CMC) and 15% SP carbon to form a slurry, which was coated onto a copper (Cu) foil with active material loading of ~1.0 mg cm^{-2} and dried in a vacuum oven at 100 °C for 10 h. Electrochemical measurements were performed with CR2032 coin-type cells assembled in an argon-filled glove box.[38] Lithium foil was used as the counter electrode and reference electrode. $LiPF_6$ (1 M) dissolved in ethylene carbonate/diethyl carbonate (EC/DEC, 1:1 by volume) was the electrolyte. Discharge-charge cycling tests were carried out in the voltage range of 0.02–3.0 V at different rates using LAND-CT2001A battery-testing system. The total mass of the Sn@C composite was used to calculate the capacity of the battery. Cyclic voltammograms (CVs) were measured in the voltage range of 0.01–3.0 V with a scan rate of 0.1 mv s^{-1} on the Parstat 263A at room temperature.

Result and discussion

Fig. 1 shows the TEM images of the as-prepared Sn8@C and Sn40@C with the comparison of the photographic cross section of pitaya. It can be clearly seen that Sn8@C and Sn40@C resemble the structure of a pitaya (Fig. 1b) with tin nanoparticle size of around 8 nm for Sn8@C (Fig. 1c) and 40 nm for Sn40@C (Fig. 1f). The proper and lower concentration of Sn8@C precursor solution (compared with Sn40@C) and the stable carbon matrix can effectively prevent Sn nanograins from growing bigger. What's more, the rapid formation of Sn@C network and high reaction temperature is considered to protect the uniform distribution of Sn@C structure during the simultaneous Sn formation and carbonization. The embedded nanostructure not only provides proper electric contact, but also acts as mechanical support to accommodate the volume change during lithiation/delithiation process. The HRTEM image in Fig. 1c shows that the tin nanograins in pitaya-like Sn8@C are around 8 nm. Fig. 1d displays a set of parallel fringes with the space of 0.298 nm, corresponding to the (200) plane of crystalline Sn (JCPDS no. 04-0673). The TEM element mapping image of Sn8@C (Fig. 1e) reveals a homogenous distribution of Sn within the composite.

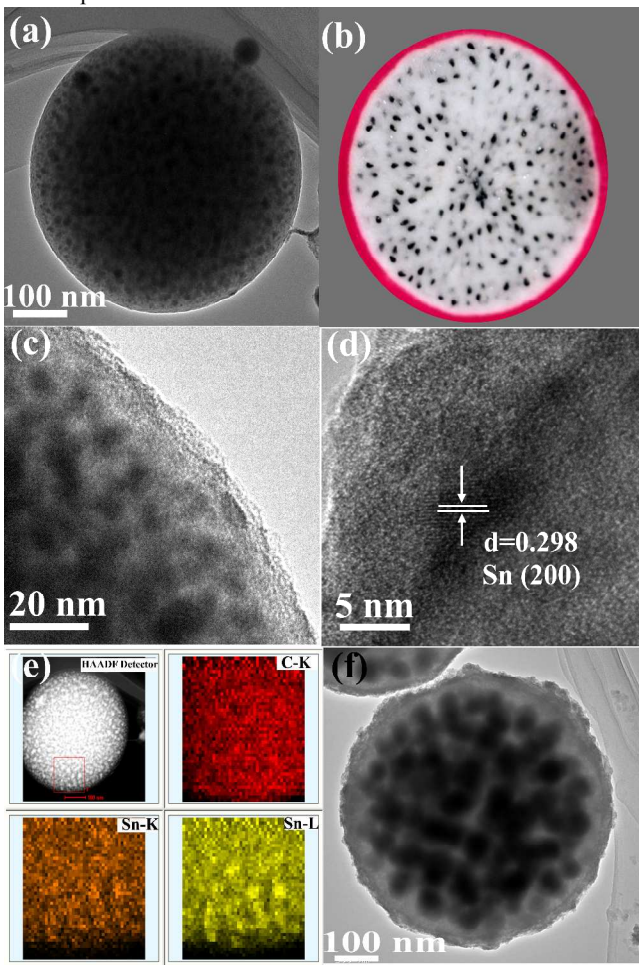

Fig. 1 (a) TEM image of Sn8@C, (b) Cross-section photograph of natural pitaya, (c, d) High-resolution TEM image of Sn8@C, (e) TEM element mapping image of Sn8@C, (f) TEM image of Sn40@C.

Fig.2 shows X-ray diffraction patterns of Sn8@C and Sn40@C. All the main peaks in the XRD patterns could be indexed to the tetragonal tin (JCPDS card no. 04-0673), while no peaks of SnO_2 or SnO were detected.

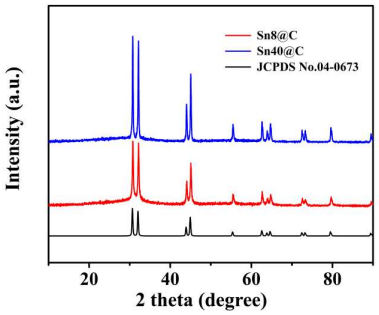

Fig. 2 XRD patterns of Sn8@C and Sn40@C nanocomposites compared with JCPDS No. 04-673.

The composition of the spherical Sn@C nanocomposite was investigated by TGA analysis in air, as shown in Fig. S3. There is only 2% weight loss observed until 220 °C, which is attributed to the elimination of adsorbed water and air. This suggests that the composite is stable in air up to 220 °C. The weight increase in the temperature range of 220 °C to 300 °C or around 350 °C is owing to the oxidation of metallic tin ($Sn + O_2 \rightarrow SnO_2$). The fast weight loss until 550 °C is attributed to the oxidation of carbon ($C + O_2 \rightarrow CO_2$ (gas)). The mass content of nano-Sn particles in Sn8@C and Sn40@C composites are 45.7% and 73.5%, respectively. It is worth to note that Sn nanoparticles in Sn8@C is ultrasmall, which induces SnO_2 reduction ($SnO_2 + C \rightarrow Sn + CO_2$) during the preparation. Furthermore, Sn8@C nanocomposite has a lower Sn content than that of Sn40@C.

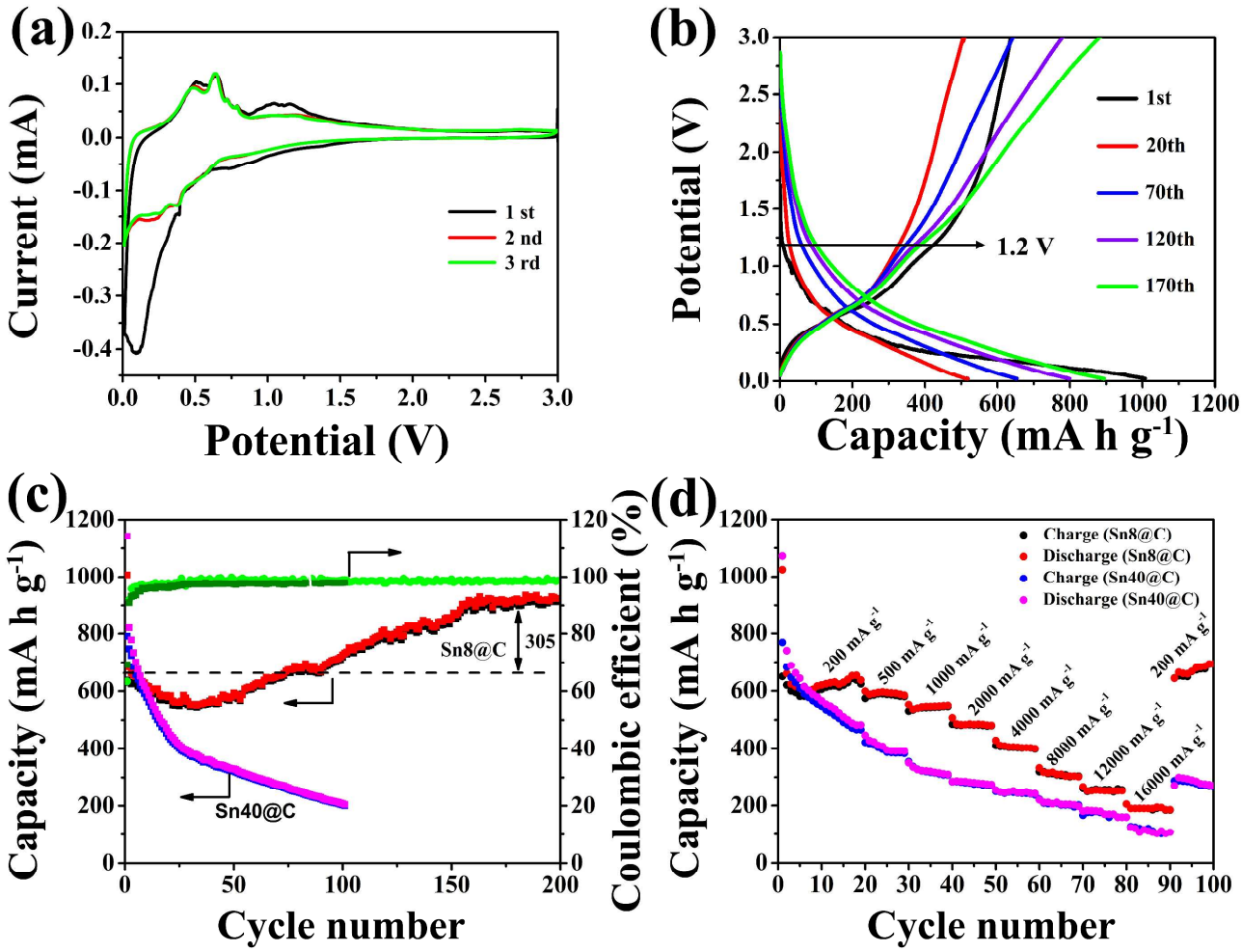

Fig. 3 (a) Cyclic voltammograms of the initial 3 cycles scanned between 0 − 3 V at a rate of 0.1 mV s^{-1} of Sn8@C, (b) Charge/discharge profiles at the 1st, 20th, 70th, 120th, 170th cycles of Sn8@C and the capacity was calculated based on the weight of Sn@C composite, (c) Cycling performance of the spherical Sn8@C and Sn40@C composites at 0.02 – 3.0 V and 200 mA g^{-1}, (d) Rate capability of Sn8@C and Sn40@C at different current densities.

Fig. 3a shows the cyclic voltammograms (CVs) of Sn8@C electrode. There are three small reduction peaks at 0.2 V, 0.4 V, and 0.55 V, revealing the formation of Li_xSn alloy. The corresponding oxidation peaks at 0.53 V, 0.68 V, and 0.78 V are assigned to delithiation reaction of Li_xSn alloy. While a broad anodic peak at 1.15 V is observed in the first cycle, which is attributed to lithium extraction from carbon. The unchanged peak current intensity (except for the first cycle) in the following cycling implies excellent reversibility of the Sn8@C nanocomposite. It should be noted that the difference between the first and the second scans corresponds to the decomposition of electrolyte to form solid-electrolyte interface (SEI) films. The CVs of the Sn40@C is shown in Fig. S4, displaying similar trend.

Fig. 3b shows the charge-discharge profiles of Sn8@C composite at a current density of 200 mA g^{-1} between 0.02 V and 3.0 V, and the charge-discharge curves of Sn40@C and pyrolyzing carbon are shown in Fig. S5 and Fig. S6a. The initial discharge and charge capacities of Sn8@C are 1007.1 mA h g^{-1} and 637.2 mA h g^{-1} with a coulombic efficiency of 63.3%. The first delithiation capacity is closed to the theoretical capacity (655 mA h g^{-1}) of Sn8@C composite (Sn : C = 45.7 : 54.3 by weight), based on the theoretical capacity of carbon (372 mA h g^{-1}) and metallic tin (992 mA h g^{-1}). The irreversible capacity loss (369.9 mA h g^{-1}) is mainly ascribed to the formation of SEI film and the electrolyte decomposition. Interestingly, the reversible capacity of Sn8@C composite increases to 910 mA h g^{-1} from the 20th cycle to the 180th cycle and subsequently stabilizes around this capacity even up to 200th cycle (Fig. 3c). The behaviour of capacity increase has been reported in SnO_2/graphene nanocomposite,[1, 39] Sn/C nanocomposite[23], Si/C composite[40] and other metal oxide systems.[41-43]

The cycling performance of Sn40@C and Sn8@C composites were evaluated under the same conditions, as shown in Fig. 3c. The Sn40@C nanocomposite shows an initial discharge capacity of 1142.7 mA h g^{-1}. Then, the capacity continuously decreases with the following 100 cycles (with only 17.9 % capacity retention). The pyrolyzing carbon shows a reversible capacity of 210 mA h g^{-1} after 20 cycles (Fig. S6b). For comparison, Sn8@C composite exhibits an excellent cycling performance. The coulombic efficiency approaches 98.5% after the 10th cycle, suggesting its high reversibility. The improved cycling performance could be attributed to two main reasons. First, the uniform embedded nanostructure and the stable carbon framework can generate a balanced stress to accommodate the large volume change and bring a strong buffering effect to prevent Sn nanoparticles from aggregating during the charge-discharge cycling. Second, the ultrasmall tin nanoparticles with the size of ~8 nm can effectively reduce the absolute stress/strain during lithiation/delithiation process. Both factors offer a synergetic coupling effect to improve the electrochemical behaviour of electrode materials.

The Sn8@C composite also shows excellent high-rate capability, as illustrated in Fig. 3d. Significantly, Sn8@C electrode can exhibit a charge/discharge capacity of 205.3 mA h g^{-1} at the current density of 16000 mA g^{-1} (24.4 C). Once the current rate returns to 200 mA g^{-1}, a stable capacity of 672 mA h g^{-1} reverts. In contrast, Sn40@C electrode only delivers 102 mA h g^{-1} at 16000 mA g^{-1} and pyrolyzing carbon shows a capacity of 85 mA h g^{-1} at 2000 mA g^{-1} (Fig. S7).

Recent studies demonstrats that the capacity increase during cycling is contributed to the reversible formation and decomposition of an organic polymeric/gel-like layer from the electrolyte.[1, 23, 41, 44] The polymeric/gel-like layer could enhance the mechanical cohesion by coating around the active materials and then provide extra lithium interfacial storage sites through a so-called "pseudo-capacitance-type behaviour".[42] As shown in Fig. 3b, the different charge–discharge profiles are plotted. The gradually increased discharge capacity at a potential above 1.2 V corresponds to the reversible decomposition of an organic polymeric/gel-like layer, which coincides with the previous reports.[23] It is believed that the organic polymeric/gel-like layer forms at low voltage and decomposes at high voltage.

Fig. 4a shows the TEM image of Sn8@C anode before decomposition, demonstrating that polymeric/gel-like layer is formed on the surface of Sn nanoparticles. Fig. 4b shows the cycling performance of Sn8@C composite at 1000 mA g^{-1}. The capacity increases from about 100 to 200 cycles in the voltage range of 0.02 V to 3.0 V, but stops increasing when cutting the charge voltage from 3.0 V to 1.5 V. This is owing to that the organic polymeric/gel-like layer is unable to decompose below 1.5 V. While, the rising trend recovers after setting the cut-off voltage back to 3.0 V. Furthermore, Fig. S8 shows the cycle performance of Sn8@C nanocomposite from the first cycle in the voltage range of 0.02 V and 1.5 V. These results indicate that the reversible formation and decomposition of an organic polymeric/gel-like layer leads to the capacity increase.

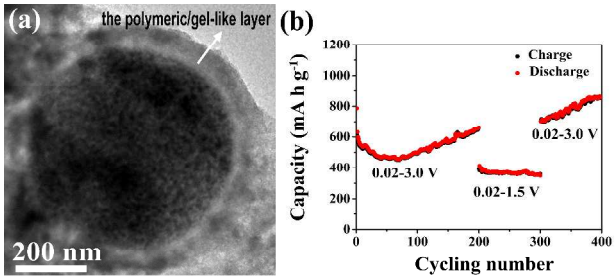

Fig. 4 (a) TEM image of spherical Sn8@C nanocomposite after charging the electrode to 1.0 V, (b) Cycling performance of the Sn8@C composite cycled at 0.02 V-3.0 V and 0.02 V-1.5 V with a current density of 1000 mA g^{-1}.

Table 1 Comparison of Sn-C composites prepared by using the same method of aerosol spray pyrolysis.

Sample	Tin/carbon sources	Surfactant and carrying gas	Tin particles size	Rate capability	Cyclability	Reference
Nano-Sn/C	$SnCl_2$; PVP	PVP; H_2/Ar	~ 10 nm	390 mA h g^{-1} at 3780 mA g^{-1}	710 mA h g^{-1} at 200 mA g^{-1} (130 cycles)	26
Sn-$C_{Pluronic}$	$SnCl_2$; sucrose Pluronic-F127	Pluronic-F127; Ar	~ 15 nm	300 mA h g^{-1} at 3000 mA g^{-1}	640 mA h g^{-1} at 500 mA g^{-1} (200 cycles)	32
Sn8@C	$SnCl_2$; resorcinol and formaldehyd	--; Ar	~ 8 nm	429.6 mA h g^{-1} at 4000 mA g^{-1}	910 mA h g^{-1} at 200 mA g^{-1} (200 cycles) 780 mA h g^{-1} at 800 mA g^{-1} (400 cycles) 410 mA h g^{-1} at 4000 mA g^{-1} (1000 cycles)	this work

Fig. 5 further illustrates the cycling performance of Sn8@C electrode conducted at 4000 mA g^{-1}. The charge/discharge capacity varies from 370 to 410 mA h g^{-1} with a high coulombic efficiency around 100%. These results demonstrate the remarkable energy density, high-rate capability, and long-term

cycling stability of Sn8@C composite. Besides, compared with the other Sn-C composites synthesized by using the same way of aerosol spray pyrolysis, Sn8@C shows a better performance (Table 1). Notably, the extent of increasing capacity at the current density of 4000 mA g^{-1} (Fig. 5) is lower than that of 200 mA g^{-1} and 800 mA g^{-1} (Fig. 3c and Fig. S9). This phenomenon is attributed to the insufficient formation and decomposition of organic polymeric/gel-like layer at a relative high current density. Moreover, the morphology and structure changes of the electrode after charge/discharge cycles were checked by TEM (Fig. 6). Fig. 6a shows that Sn8@C composite still sustains the uniform spherical shape after 1000 discharge/charge cycles at 4000 mA g^{-1}. This suggests that the ultrasmall Sn nanoparticles and a stable embedded carbon matrix of Sn8@C can effectively alleviate the large volume change and curb the pulverization and aggregation of Sn nanoparticles. In contrast, after 100 discharge/charge cycles, the spherical structure of Sn40@C composite collapses and partly Sn particles pulverizes with aggregation (Fig. 6b).This can answer why the Sn8@C nanocomposite could have the amazing cycling performance.

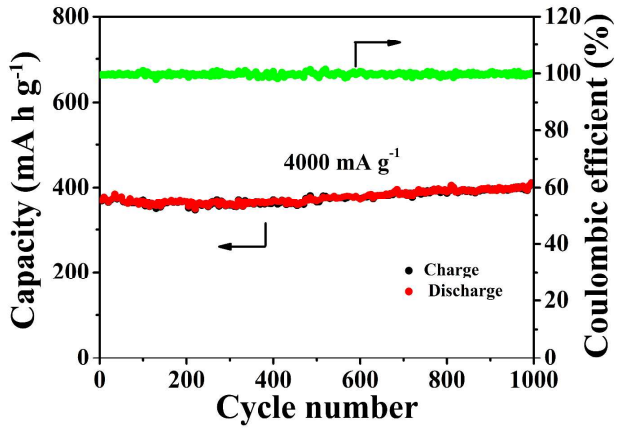

Fig.5 Cycling performance of Sn8@C at the current density of 4000 mA g^{-1} between 0.02 V and 3.0 V.

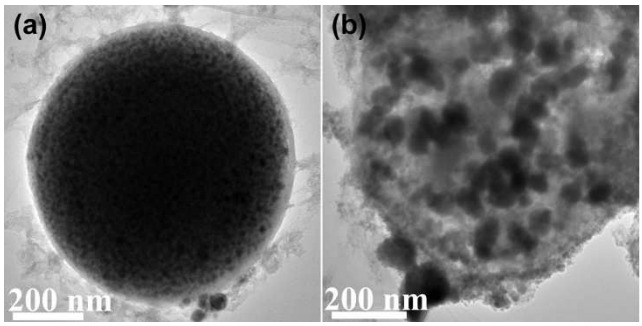

Fig.6 (a) TEM image of Sn8@C composite after 1000 discharge and charge cycles at 4000 mA g^{-1}; (b) TEM image of Sn40@C composite after 100 discharge and charge cycles at 200 mA g^{-1}.

Conclusions

Pitaya-like Sn@C nanocomposites with Sn nanoparticles (about 8 nm and 40 nm) uniformly dispersed in the carbon matrix were successfully fabricated by an aerosol spray pyrolysis method. The size of the embedded Sn nanoparticles can be controlled through changing the concentration of the raw material. With the application as anode material for lithium–ion batteries, the as-prepared Sn8@C nanocomposite shows a charge/discharge capacity of 410 mA h g^{-1} up to 1000 cycle at 4000 mA g^{-1} (6.1 C). The capacity of 205.3 mA h g^{-1} was observed even at a high current density of 16000 mA g^{-1} (24.4 C). This high-rate electrochemical performance is attributed to the uniform dispersion of ultrasmall Sn nanoparticles in spherical carbon matrix with a buffered structure. The simplified preparation process and the high electrochemical performance of Sn8@C composite make it promising in the application as the anode materials for lithium-ion batteries.

Acknowledgements

This work was supported by the Programs of National 973 (2011CB935900), NSFC (51231003), 111 Project (B12015) and the Fundamental Research Funds for the Central Universities.

Notes and references

Key Laboratory of Advanced Energy Materials Chemistry (Ministry of Education), College of Chemistry, Nankai University, Tianjin 300071, China; Collaborative Innovation Center of Chemical Science and Engineering, Tianjin 300071, China, Fax: 86-22-23509571; Tel: 86-22-23506808.

E-mail: chenabc@nankai.edu.cn

† Electronic Supplementary Information (ESI) available: Schematic of the aerosol spray pyrolysis platform, SEM images of different Sn@C samples, TGA curves, Cyclic voltammograms of Sn40@C, Charge/discharge profiles of Sn40@C, Electrochemical performance of pyrolyzing carbon, Cycling performance of Sn8@C from the frist cycle between 0.02 V and 1.5 V, Cycling performance of Sn8@C at 800 mA g^{-1}. See DOI: 10.1039/b000000x/

1. D. N. Wang, J. L. Yang, X. F. Li, D. S. Geng, R. Y. Li, M. Cai, T. K. Sham and X. L. Sun, *Energy Environ. Sci.*, 2013, **6**, 2900-2906.
2. Y. Qiu, K. Yan and S. Yang, *Chem. Commun.*, 2010, **46**, 8359-8361.
3. Z. Tan, Z. H. Sun, H. H. Wang, Q. Guo and D. S. Su, *J. Mater. Chem. A*, 2013, **1**, 9462-9468.
4. D. Deng and J. Y. Lee, *Angew. Chem. Int. Ed.*, 2009, **48**, 1660-1663.
5. G. Derrien, J. Hassoun, S. Panero and B. Scrosati, *Adv. Mater.*, 2007, **19**, 2336-2340.
6. B. Peng and J. Chen, *Coord. Chem. Rev.*, 2009, **253**, 2805-2813.
7. F. Y. Cheng, J. Liang, Z. L. Tao and J. Chen, *Adv. Mater.*, 2011, **23**, 1695-1715.
8. A. H. Lim, H. W. Shim, S. D. Seo, G. H. Lee, K. S. Park and D. W. Kim, *Nanoscale*, 2012, **4**, 4694-4701.
9. B. J. Landi, M. J. Ganter, C. D. Cress, R. A. DiLeo and R. P. Raffaelle, *Energy Environ. Sci.*, 2009, **2**, 638-654.
10. K. T. Lee, Y. S. Jung and S. M. Oh, *J. Am. Chem. Soc.*, 2003, **125**, 5652-5653.
11. R. Z. Hu, H. Liu, M. Q. Zeng, J. W. Liu and M. Zhu, *J. Mater. Chem.*, 2012, **22**, 9539-9545.
12. J. Chen and F. Y. Cheng, *Acc. Chem. Res.*, 2009, **42**, 713-723.
13. L. F. Cui, J. Shen, F. Y. Cheng, Z. L. Tao and J. Chen, *J. Power Sources*, 2011, **196**, 2195-2201.
14. H. Mukaibo, T. Sumi, T. Yokoshima, T. Momma and T. Osaka, *Electrochem. Solid-State Lett.*, 2003, **6**, A218-A220.

15. X. L. Wang, W. Q. Han, J. Chen and J. Graetz, *ACS Applied Materials & Interfaces*, 2010, **2**, 1548-1551.
16. R. Z. Hu, M. Zhu, H. Wang, J. W, Liu, L. Z. OuYang and J. Zou, *Acta Mater*, 2012, **60**, 4695-4703.
17. R. Z. Hu, H. Liu, M. Q. Zeng, H. Wang and M. Zhu, *J. Mater. Chem*., 2011, **21**, 4629-4635.
18. C. Zhai, N. Du, H. Zhang, J. Yu, P. Wu, C. Xiao and D. Yang, *Nanoscale*, 2011, **3**, 1798-1801.
19. Y. Liang, Z. G. Tian, Y. Liu and Y. S. Luo, *J. Phys. Chem. Solids*, 2009, **70**, 79-83.
20. L. Y. Beaulieu and J. R. Dahn, *J. Electrochem. Soc.*, 2000, **147**, 3237-3241.
21. Y. Wang, J. Y. Lee and T. C. Deivaraj, *J. Electrochem. Soc.*, 2004, **151**, A1804-A1809.
22. Y. H. Xu, Q. Liu, Y. J. Zhu, Y. H. Liu, A. Langrock, M. R. Zachariah and C. S. Wang, *Nano Lett.*, 2013, **13**, 470-474.
23. Y. Xu, J. Guo and C. Wang, *J. Mater. Chem.*, 2012, **22**, 9562-9567.
24. D. N. Wang, X. F. Li, J. L. Yang, J. J. Wang, D. S. Geng, R. Y. Li, M. Cai, T.-K. Sham and X. L. Sun, *Phys. Chem. Chem. Phys*., 2013, **15**, 3535-3542.
25. Y. Yu, L. Gu, C. Zhu, P. A. van Aken and J. Maier, *J. Am. Chem. Soc.*, 2009, **131**, 15984-15985.
26. Y. Yu, C. H. Chen and Y. Shi, *Adv. Mater.*, 2007, **19**, 993-997.
27. X. F. Song, *Nanotechnology*, 2013, **24**, 205401-205407.
28. F. Y. Cheng and J. Chen, *J. Mater. Res.*, 2006, **21**, 2744-2757.
29. J. Guo, Z. Yang and L. A. Archer, *J. Mater. Chem. A*, 2013, **1**, 8710-8715.
30. C. Boissiere, D. Grosso, A. Chaumonnot, L. Nicole and C. Sanchez, *Adv. Mater.*, 2011, **23**, 599-623.
31. Q. Xiao, H. Sohn, Z. Chen, D. Toso, M. Mechlenburg, Z. H. Zhou, E. Poirier, A. Dailly, H. Wang, Z. Wu, M. Cai and Y. Lu, *Angew. Chem. Int. Ed.*, 2012, **51**, 10546-10550.
32. Y. Yan, F. Zhang, Y. Meng, B. Tu and D. Y. Zhao, *Chem. Commun*., 2007, 2867-2869.
33. N. E. Motl, A. K. P. Mann and S. E. Skrabalak, *J. Mater. Chem. A*, 2013, **1**, 5193-5202.
34. F. Y. Cheng, W. Tang, C. S. Li, J. Chen, H. K. Liu, P. S. Wen and S. X. Dou, *Chem. Eur. J*. 2006, **12**, 3082-3088.
35. N. Li, Q. Zhang, J. Liu, J. Joo, A. Lee, Y. Gan and Y. D. Yin, *Chem. Commun*., 2013, **49**, 5135-5137.
36. J. Chen, L. N. Xu, W. Y. Li and X. L. Gou, *Adv. Mater.*, 2005, **17**, 582-586.
37. F. Y. Cheng, J. Shen, B. Peng, Y. D. Pan, Z. L. Tao and J. Chen, *Nat. Chem.*, 2011, **3**, 79-84.
38. X. L. Zhang, F. Y. Chen, J. G Yang and J. Chen, *Nano Lett.,* 2013, **13**, 2822-2825.
39. P. Lian, X. Zhu, S. Liang, Z. Li, W. Yang and H. Wang, *Electrochim. Acta*, 2011, **56**, 4532-4539.
40. A. Magasinski, P. Dixon, B. Hertzberg, A. Kvit, J. Ayala and G. Yushin, *Nat. Mater.*, 2010, **9**, 461-461.
41. Z. Wang, D. Luan, S. Madhavi, Y. Hu and X. W. Lou, *Energy Environ. Sci.*, 2012, **5**, 5252-5256.
42. S. Laruelle, S. Grugeon, P. Poizot, M. Dollé, L. Dupont and J. M. Tarascon, *J. Electrochem. Soc.*, 2002, **149**, A627-A634.
43. Z. Wang, J. S. Chen, T. Zhu, S. Madhavi and X. W. Lou, *Chem. Commun.*, 2010, **46**, 6906-6908.
44. W. Wei, S. Yang, H. Zhou, I. Lieberwirth, X. Feng and K. Müllen, *Adv. Mater.*, 2013, **25**, 2909-2914.

TOC

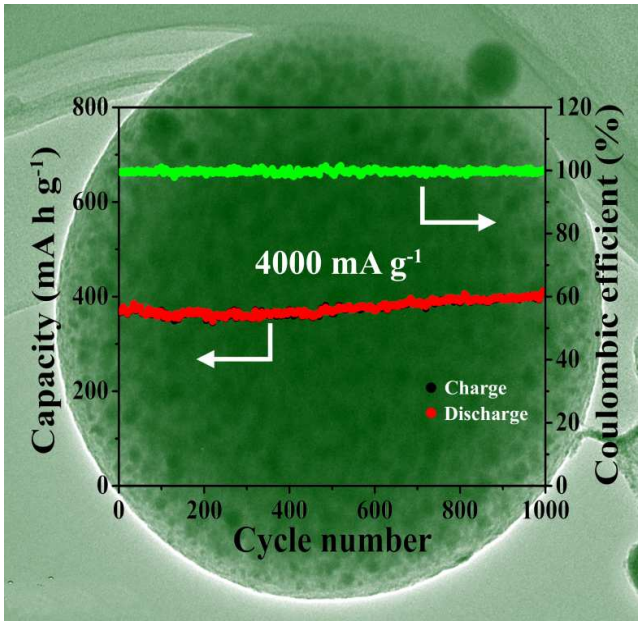

As the anode material of lithium-ion batteries, pitaya-like Sn8@C nanocomposite shows the reversible capacity of 410 mA h g^{-1} after 1000 cycles at 4000 mA g^{-1} in the voltage range of 0.02 V and 3.0 V.